TABLE 1 Excitation Voltage and Input Impedance of the Array Synthesized in Figure 3

Array Element	Voltage (V)	Impedance (Ω)
1–20	$0.89 \cdot e^{j \cdot 1.28}$	$53.4 + j \cdot 17.8$
2–19	$1.32 \cdot e^{j \cdot 0.89}$	$59.0 - j \cdot 2.0$
3–18	$1.97 \cdot e^{j \cdot 1.08}$	$52.8 + j \cdot 5.5$
4–17	$3.01 \cdot e^{j \cdot 1.03}$	$63.2 + j \cdot 4.5$
5–16	$4.04 \cdot e^{-j \cdot 1.87}$	$63.5 + j \cdot 23.0$
6–15	$5.40 \cdot e^{-j \cdot 2.78}$	$61.5 + j \cdot 32.5$
7–14	$6.26 \cdot e^{-j \cdot 1.18}$	$55.2 + j \cdot 33.3$
8–13	$6.97 \cdot e^{j \cdot 0.33}$	$59.2 + j \cdot 26.1$
9–12	$7.15 \cdot e^{j \cdot 1.08}$	$48.6 + j \cdot 9.5$
10–11	$7.71 \cdot e^{j \cdot 1.02}$	$56.5 + j \cdot 5.7$

excitations of the array elements have been obtained by the proposed synthesis procedure. In the same way as in the previous example, the radiation of the array in the presence of the platform and its own array elements has been modeled with the MoM. It can be seen that the synthesized array clearly satisfies the SLL requirement of 40 dB in the whole angular margin, showing a very good agreement with the objective pattern. For the sake of completeness, the excitation voltage and the input impedance of each array element in this example are summarized in Table 1; as expected, both the impedance and the excitation are symmetric for this particular case.

Finally, in order to illustrate the scanning capabilities of the proposed method, Figure 4 shows a new objective pattern with the maximum displaced from the broadside direction and the respective radiation pattern obtained when the array has been synthesized by the proposed method. As in previous results, all of the electromagnetic couplings involved in the problem have been modeled with the MoM and included in the numerical results. Once again, a very good agreement with the objective pattern can be observed.

4. CONCLUSIONS

Conformal array antennas attached to real complex platforms are synthesized in order to obtain low-sidelobe radiation platforms. A previous technique has been improved and extended to 3-D problems throughout an efficient method-of-moments formulation. The inclusion of array elements attached to the structure, whose electromagnetic coupling with the structure is very strong, has been successfully addressed in this paper. Numerical results have shown that high-performance radiation patterns (even with scanning capabilities) for onboard array antennas can be easily achieved. Even though the formulation has been stated for perfect electric conducting structures, it could be easily extended to dielectric bodies using the adequate method-of-moments formulation for this kind of geometry.

REFERENCES

1. H. Steyskal, Synthesis of antenna patterns with imposed near-field nulls, Electron Lett 30 (1994), 2000–2001.
2. L. Landesa, F. Obelleiro, J.L. Rodríguez, J.A. Rodríguez, F. Ares, and A.G. Pino, Pattern synthesis of array antennas with additional isolation of near-field arbitrary objects, Electron Lett 34 (1998), 1540–1542.
3. L. Landesa, F. Obelleiro, J.L. Rodríguez, and A.G. Pino, Pattern synthesis of array antennas in presence of conducting bodies of arbitrary shape, Electron Lett 33 (1997), 1512–1513.
4. F. Obelleiro, L. Landesa, J.L. Rodríguez, A.G. Pino, and M.R. Pino, Directivity optimisation of an array antenna with obstacles within its near-field region, Electron Lett 33 (1997), 2087–2088.
5. L. Landesa, J.M. Taboada, F. Obelleiro, and J.L. Rodríguez, Design of on-board array antennas by pattern optimization, Microwave Opt Technol Lett 21 (1999), 446–448.
6. G.J. Burke and A.J. Poggio, Numerical electromagnetic code—Method of moments, tech document 116, AFWL-TR-76-320, Naval Ocean Systems Center, 1997.
7. R.F. Harrington, Field computation by moment method, IEEE Press, New York, 1993.
8. S.M. Rao, D.R. Wilton, and A.W. Glisson, Electromagnetic scattering by surfaces of arbitrary shape, IEEE Trans Antennas Propagat AP-30 (1982), 409–418.
9. S.U. Hwu and D.R. Wilton, Electromagnetic scattering and radiation by arbitrary configurations of conducting bodies and wires, San Diego State University, tech rep 87-17, May 1998.
10. J.M. Taboada, J.L. Rodríguez, and F. Obelleiro, Comparison of moment-method solutions for wire antennas attached to arbitrarily shaped bodies, Microwave Opt Technol Lett 26 (2000), 413–419.

PERFORMANCE TOLERANCE IN MICROPRISM-TYPE BENT WAVEGUIDES

Jui-Ming Hsu[1] and Ching-Ting Lee[1]
[1] Institute of Optical Sciences
National Central University
Chung-Li 32054, Taiwan, R.O.C.

Received 19 December 2000

ABSTRACT: *By taking into account the inevitable fabrication tolerance, we present two kinds of performance-tolerant models for microprism-type bent waveguides. The optical transmitted power efficiency is investigated by using the fast Fourier transform beam propagation method and the orthogonality overlap integral. We demonstrate the dependence of the performance tolerance region on practical fabrication parameters.* © 2001 John Wiley & Sons, Inc. Microwave Opt Technol Lett 29: 328–332, 2001.

Key words: *integrated optics; bent waveguide; optical waveguides; prisms; performance tolerance*

1. INTRODUCTION

To achieve a wide-angle and low-loss bent waveguide, the microprism-type bent waveguide [1–5] has the most potential for practical application in a variety of reported structures [1–7]. We have systematically derived precise phase compensation formulas for the design of microprism-type bent waveguides [1]. According to our reported microprism-type structures [1], an ideal microprism with a higher index placed at the bent corner was designed to exactly compensate for the phase difference between the phase fronts in front of and behind the bent region, whereby the bending loss was reduced significantly. However, the vertices of the designed microprism shape are distorted and flattened during practical fabrication processes. Furthermore, the accurate refractive indexes of the designed structure are unattainable in the practical deposition fabrication. The flattened vertex and

Contract grant sponsor: National Science Council, Republic of China
Contract grant number: NSC 89-2215-E008-009

variant index would degrade the bending loss for the ideal microprism shape. Therefore, experiential values of the inevitable fabrication tolerance on the flattened vertex and variant index are beneficial to the design of microprism-type bent waveguide structures.

In this letter, to study the dependence of performance degradation on the fabrication tolerance, we construct two kinds of tolerance models for the flattened vertex and variant index, respectively. By applying the fast Fourier transform beam propagation method (FFT–BPM) [8] and an orthogonality overlap integral based on the orthogonality principal [9–10] to these two models, the transmitted power efficiencies of the two tolerance models are simulated. Finally, the dependences of the performance tolerance range on inevitable fabrication parameters can be used as a design guide for microprism-type bent waveguides.

2. TOLERANCE MODEL

The top view of an embedded microprism-type abrupt bent waveguide and its three dimensional (3-D) structure are shown in Figure 1(a) and (b), respectively. A transverse-electric (TE) single-mode beam with a waveguide $\lambda = 1.5$ μm is coupled into the left facet of the waveguide shown in Figure 1(a). The geometric and dielectric parameters are chosen to be the same as in our previous report [1] for the study here: waveguide with $W_g = 9$ μm, waveguide thickness $H_g = 6.9$ μm, and refractive indexes $n_s = 1.5$, $n_g = 1.504$, and $n_p = 1.6$ for the substrate, waveguide, and microprism, respectively. The analytic domain is chosen as the transverse with $L_x = L_y = 60\lambda$ and propagation distance $L_z = 260$ μm, which is composed of a 60 μm straight waveguide and an oblique waveguide with 200 μm projection. The step sizes in the propagation and transverse directions are $\Delta z = 0.5$ μm and $\Delta x = \Delta y = 60\lambda/128$, respectively. Since the microprism width W_p and depth H_p should be large enough to confine most of the optical power, they are respectively chosen as $2W_g$ and $2H_g$ in this study.

By means of the phase compensation method proposed in our previous report [1], the phase difference $\Delta\phi_b$ between the inner curve path AB and the outer curve path $A'B'$ in the bent region without a microprism is equal to the corresponding phase difference $\Delta\phi_p$ contributed by the microprism. Therefore, the relation between the refractive index of microprism n_p and the parameters of the bent waveguide is written as

$$(n_p - n_s)\frac{(W_A - W_p)}{2}\left[\frac{\cos(\theta/2) - m\cos^2(\theta/2)}{1 - m\cos^2(\theta/2)}\right] = n_s W_p \tag{1}$$

where θ is the bent angle, W_A is the width of the analytic space of the bent region, and $m = (W_A - W_p)/(W_A + W_p)$. Using this microprism-type bent waveguide structure, we construct a tolerance model for the flattened vertex and variant index as follows. To simplify this simulation, when one of the two models is simulated, the other model is kept in the designed ideal situation.

2.1. Flattened-Vertex Tolerance Model. We model a bent waveguide structure with a microprism whose vertices are distorted and flattened as shown in Figure 2(a). For the sake of convenience, we denote V_o and V_i as the vertex of the microprism which, respectively, locate at the outermost and innermost optical paths as shown in Figure 2(a). The vertices of the microprism may be truncated with the flattening extent Δ_o and Δ_i for the photolithography process, which are defined as the distance between the vertices and the truncated facets with respect to V_o and V_i.

Generally, the radiation modes exist in the effective waveguide with W_{eff} region when they propagate along the oblique waveguide. Therefore, the transmitted power efficiency would be overevaluated due to the inaccurate consideration of the total power within the W_{eff} region as transmitted power. To exclude the radiation modes within the W_{eff} region, the

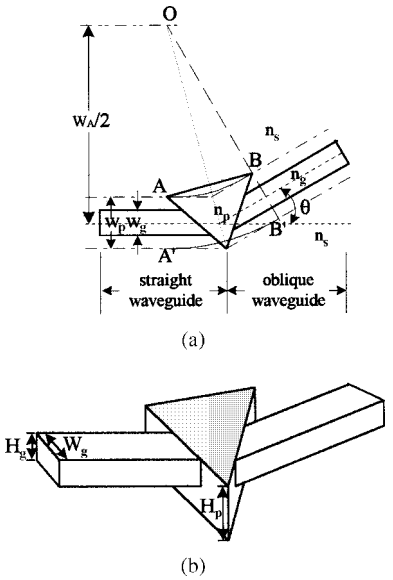

Figure 1 Microprism-type bent waveguide. (a) Top view. (b) Three-dimensional structure

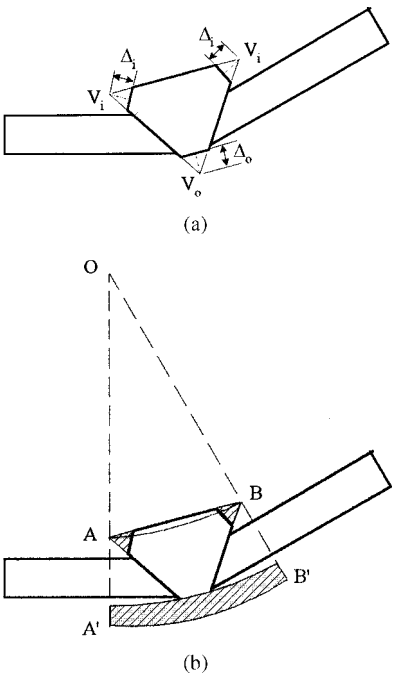

Figure 2 (a) Vertex-flattened model of microprism-type bent waveguide. (b) Phase compensation is affected by outer and inner flattened vertices

orthogonality overlap integral based on the orthogonality principle [9–10] is used to calculate the transmitted power efficiency in this study. The normalized optical power P_i at the input end ($z = 0$) is given by

$$P_i = \frac{\left| \iint_{L_x, L_y} \phi(x, y, 0) f(x, y, 0)\, dx\, dy \right|^2}{\iint_{L_x, L_y} |\phi(x, y, 0)|^2 dx\, dy \iint_{L_x, L_y} |f(x, y, 0)|^2 dx\, dy}. \tag{2}$$

The optical field $f(x, y, 0)$ at the input end is just the injected eigenmode $\phi(x, y, 0)$. At the output end ($z = L_z$), the normalized optical power P_o is given by

$$P_o = \frac{\left| \iint_{L_x, L_y} \phi'(x', y, L_z) f(x', y, L_z)\, dx\, dy \right|^2}{\iint_{L_x, L_y} |\phi'(x', y, L_z)|^2 dx\, dy \iint_{L_x, L_y} |f(x', y, L_z)|^2 dx\, dy} \tag{3}$$

where $f(x', y, L_z)$ is the optical field at the output end, and the eigenfield located at the output end $\phi'(x', y, L_z)$ can be expressed as $\phi'(x', y, L_z) = \phi(x \cos\theta, y, 0) \exp(j\beta x \sin\theta)$ for a propagation constant β by adopting a coordinate transformation.

The transmitted power efficiency η is defined as the ratio of the output and input normalized optical powers, i.e.,

$$\eta = \frac{P_o}{P_i}. \tag{4}$$

Substantially, the optical field $f(x', y, L_z)$ is a composite of the guided and residual radiation modes. Referring to the orthogonality property, for the numerator in Eq. (3), the integral of the products of the eigenfields $\phi'(x', y, L_z)$ and the radiation components of the optical fields $f(x', y, L_z)$ is zero. Therefore, as mentioned previously, the radiation power is excluded from the η-estimation.

By using the FFT–BPM and orthogonality overlap integral, we can estimate the transmitted power efficiency η due to the vertex-flattened effects caused by Δ_o, Δ_i, or both Δ_o and Δ_i. By means of these simulation results, we can obtain the dependence of performance tolerance on the fabrication tolerance of the flattened-vertex tolerance model. Furthermore, we can compare the degrading sensitivity of the vertex-flattened effects caused by Δ_o and Δ_i.

2.2. Variant-Index Tolerance Model. For the practical fabrication process, the waveguide and microprism can be constructed from the silicon–oxide composite material SiO_x. By suitably controlling the deposition variables, such as temperature, pressure, and reactant concentration, the x-value of the resultant SiO_x is changed from 0 to 2 [11]. Therefore, the associated refractive index of the SiO_x can be changed from 3.4 (Si) to 1.46 (SiO_2) [12]. For the practical fabrication of the structure as shown in Figure 1(a) and (b), a glass or other substrate with a refractive index of n_s (1.5) can be used. A silicon–oxide composite material with thickness H_p and refractive index n_s was deposited. After wet etching the deposited film in the waveguide region by using a standard photolithography technique, the waveguide material with a refractive index of n_g (1.504) was then deposited. Similarly, by using the same photolithography technique and etching the microprism region, the microprism of n_p can be deposited. The deposition uncertainty in the practical fabrication process causes the refractive indexes to be different from the designed values. Therefore, the index uncertainties cause the η-degradation of the microprism-type bent waveguide. To study the influence of the index uncertainties on the microprism-type bent waveguide, we select a set of suitable index variances Δn, and let $n_i \pm \Delta n$ instead of the designed n_i, where n_i represents n_g, n_s, or n_p, respectively. Applying the FFT–BPM and orthogonality overlap integral, we estimate the dependence of the normalized transmitted power efficiency η_o on $n_i \pm \Delta n$. In order to simplify the simulation, when one of the variant refractive indexes is simulated, the other two indexes are maintained as the designed value. According to the simulated result, we can obtain the dependence of performance degradation on the fabrication tolerance of the variant-index tolerance model.

3. NUMERICAL RESULTS AND DISCUSSIONS

In our opinion, the vertex-flattened effect of the outer vertex is more sensitive than the inner vertices. This can be explained as follows. The phase difference between the outer optical curve path $A'B'$ and the inner optical curve path AB shown in Figure 1(a) is exactly compensated by an intact microprism [1]. If the outer vertex is now flattened, several optical paths, which are symboled as the shadowed curved zone region shown in Figure 2(b), will be out of compensation. On the other hand, the inner optical path lengths in the small shadowed triangular regions are missed when the inner vertices are flattened. Comparing these two kinds of vertex-flattened cases, the former one is obviously more serious than the latter one.

For the sake of conciseness, we select one bent angle $\theta = 10°$ to simulate the performance tolerance. By using the same method, the performance tolerance of the other bent angle can be simulated. Figure 3(a) and (b) shows the performance tolerance of the flattened vertex for outer and inner vertex-flattened case, respectively. The optical power efficiency η is estimated at the output facet, which is 260 μm from the input facet, shown in Figure 1(a). Referring to our geometric parameters, the flattening extent $\Delta = 5$ μm is large enough for the fabrication tolerance of microprisms in a practical technique. Therefore, we use $\Delta = 5$ μm as an uppermost flattening extent in our simulation. To construct a design guidance for the fabrication tolerance, we must select a reasonable tolerance range in the numeric results. The transmitted power efficiency degradation of 5% from the ideal case (i.e., $\Delta_o = 0$ μm and $\Delta_i = 0$ μm) of normalized efficiency $\eta_o = 100\%$ is defined as the limitation of performance tolerance, and is called "5% tolerance" in this study. As shown in Figure 3(a), the corresponding flattening extent of the outer vertex-flattened case for the 5% down power efficiency is $\Delta_o = 3.64$ μm. Therefore, the 5% tolerance of the outer vertex-flattened case is caused from $\Delta_o = 0$ to $\Delta_o = 3.64$ μm. In other words, to keep the normalized transmitted power efficiency larger than 95%, one must control the fabrication flattened error within 3.64 μm. Figure 3(b) reveals that the normalized transmitted power efficiency for the inner vertex-flattened case is $\eta_o = 97.88\%$, even though Δ_i is as large as 5 μm. Figure 3(c) compares the dependence of performance degradation on the fabrication tolerance of

these two kinds of vertex-flattened cases. As anticipated, the vertex-flattened effect of the outer vertex-flattened case is more serious than the inner vertex-flattened one. For a more practical case (we call it a "hybrid case" in this letter), both the outer and inner vertices are flattened in the fabrication process. In order to simplify the simulation, assume that the flattening extent for each of the three vertices is identical and symbolized as Δ in the hybrid case. Figure 4 shows the dependence of performance degradation on the fabrication tolerance of the hybrid case. It can be seen that the 5% tolerance of the hybrid case is caused from $\Delta = 0$ to $\Delta = 3.44\ \mu$m, and the tolerance is slightly stricter than the outer vertex-flattened case. By comparing Figure 3(a) with Figure 4, we can verify again that the influence of the inner vertex-flattened effect is quite slight.

Figure 5(a)–(c) shows the dependence of performance degradation on the index-variant fabrication tolerances of the microprism, waveguide, and substrate, respectively. The distribution of η_o is almost symmetric for n_p in Figure 5(a), and the peak normalized transmitted power efficiency η_o = 100% for the ideal index $n_p = 1.6000$. As shown in this figure, the refractive indexes of microprism n_p corresponding to the 5% down transmitted power efficiency $\eta_o = 95\%$ are $n_p = 1.5942$ and $n_p = 1.6066$, respectively. Therefore, the 5%

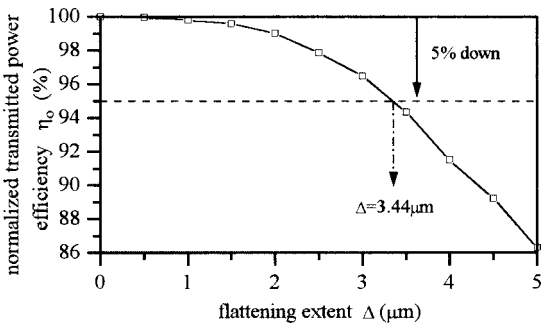

Figure 4 Dependences of normalized transmitted power efficiency η_o on the flattening extent Δ for both flattened inner and outer vertices with bent angle $\theta = 10°$

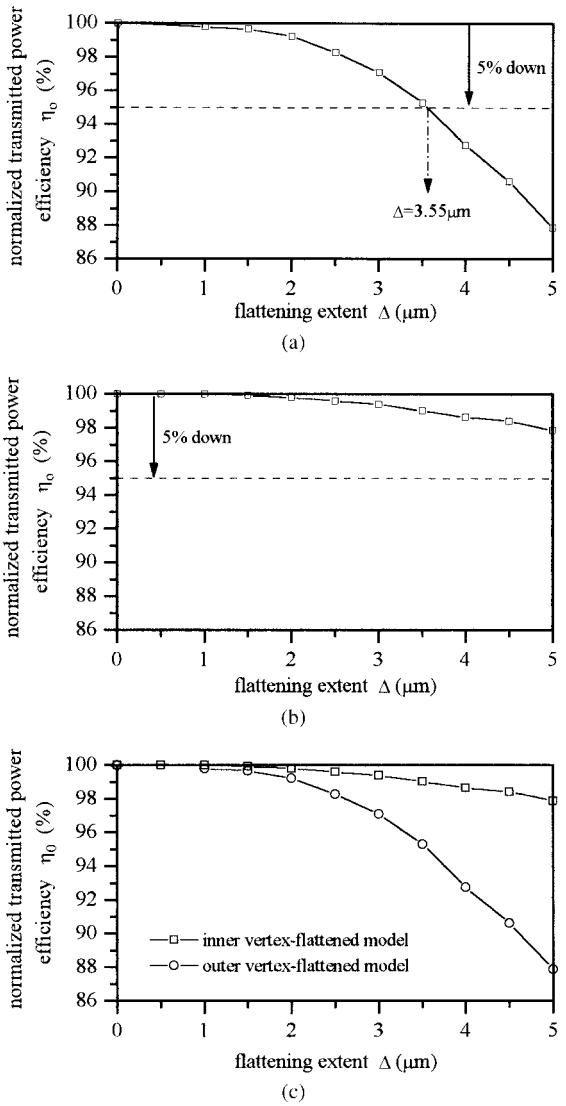

Figure 3 Dependences of normalized transmitted power efficiency η_o on the flattening extent Δ for (a) flattened outer vertex only, (b) flattened inner vertices only, (c) comparison of the η_o of (a) and (b) with bent angle $\theta = 10°$

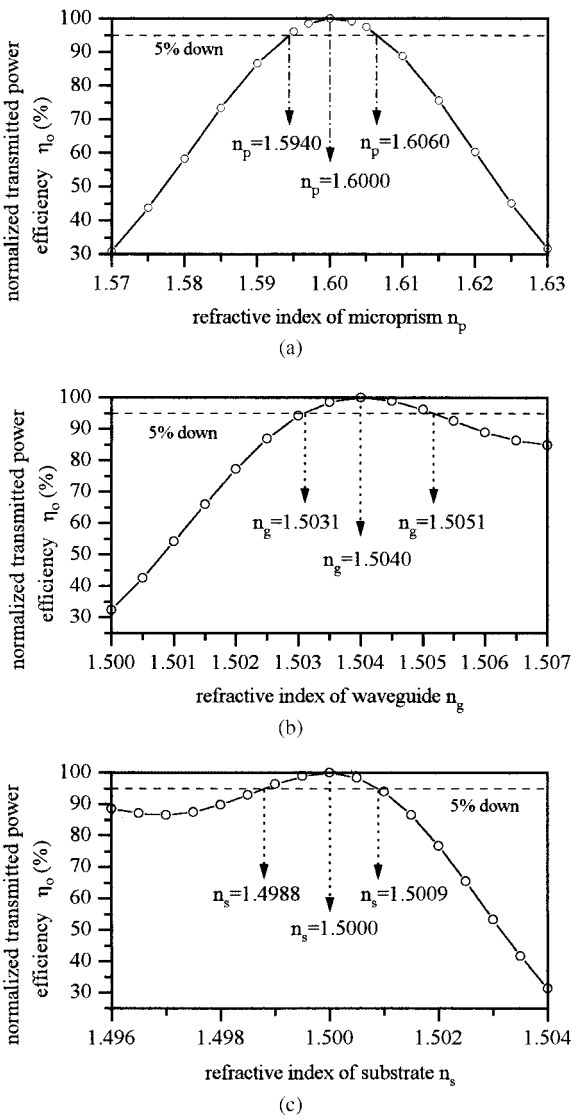

Figure 5 Dependences of normalized transmitted power efficiency η_o on the variant refractive indexes for (a) microprism, (b) waveguide, and (c) substrate with bent angle $\theta = 10°$

tolerance of the microprism-index-variant case is caused from $n_p = 1.5942$ to $n_p = 1.6066$. In Figure 5(b), the peak normalized transmitted power efficiency $\eta_o = 100\%$ is achieved for our design index of $n_g = 1.5040$. The 5% tolerance of the waveguide-index-variant case, which is estimated to be the same as mentioned above, is caused from $n_g = 1.5030$ to $n_g = 1.5052$. It is worth noting that the degradation of η in the smaller n_g is steeper than the larger one. This phenomenon can be explained as follows. The normalized frequency V, referred to as the V-parameter, is defined as [13]

$$V = k_o W_g \sqrt{n_g^2 - n_s^2} \tag{5}$$

where k_o is the wavenumber in free space. According to Eq. (5), the smaller the difference of n_g and n_s, the smaller the V-parameter. Generally, the smaller the V-parameter, the worse the confinement. In Figure 5(b), for a fixed index of the substrate $n_s = 1.5000$, the smaller n_g causes a smaller difference of n_g and n_s. Therefore, η_o degrades quickly at the smaller part of n_g. Similarly, in Figure 5(c), the peak normalized transmitted power efficiency $\eta_o = 100\%$ is achieved for our design index of $n_s = 1.5000$. The 5% tolerance of the substrate-index-variant case is caused from $n_s = 1.4987$ to $n_s = 1.5009$. As shown in this figure, the degradation of η_o in the larger n_s is steeper than the smaller one. This phenomenon is contrarily compared with Figure 5(b), and can be clearly explained using Eq. (5). For a fixed index of waveguide $n_g = 1.5040$, the larger n_s results in a smaller difference of n_g and n_s. Therefore, η_o degrades quickly at the larger part of n_s.

4. CONCLUSIONS

In this letter, we have constructed two kinds of performance-tolerant models of a microprism-type bent waveguide for the first time in the literature. By using a FFT–BPM and orthogonality overlap integral, the transmitted power efficiencies of the two types of fabrication tolerance are estimated. We defined a 5% tolerance as a tolerance limitation, and simulated several kinds of fabrication-tolerant cases. Although only the dependences of the transmission efficiency on the distortion of the microprism shape and material variation for a single bent angle $\theta = 10°$ were studied here, the performance tolerance caused by the other inevitable fabrication parameters and the other bent angle can be systematically investigated using our proposed method. Moreover, the dependence of the performance tolerance on the complex fabrication tolerance simultaneously caused from both the flattened vertex and variant index can also be investigated. This study can be adopted as a useful design guide for practical microprism-type bent waveguides.

REFERENCES

1. C.T. Lee and J.M. Hsu, Systematic design of microprism-type low-loss step-index bent waveguides, Appl Opt 37 (1998), 3948–3953.
2. S.K. Korotky, E.A.J. Marcatili, J.J. Veselka, and R.H. Bosworth, Greatly reduced losses for small-radius bends in Ti:LiNbO3 waveguides, Appl Phys Lett 8 (1986), 92–94.
3. K. Hirayama and M. Koshiba, A new low-loss structure of abrupt bend in dielectric waveguides, J Lightwave Technol 10 (1992), 563–569.
4. P.L. Fan, M.L. Wu, and C.T. Lee, Analysis of abrupt bent waveguides by the beam propagation method and the conformal mapping method, J Lightwave Technol 15 (1997), 1026–1031.
5. C.T. Lee and P.L. Fan, Beam propagation analysis of fast mode-conversion evolution bent waveguides with apexes-linked microprisms, IEEE Microwave Guided Wave Lett 7 (1997), 338–340.
6. T. Shiina, K. Shiraishi, and S. Kawakami, Waveguide-bend configuration with low-loss characteristics, Opt Lett 11 (1986), 736–738.
7. M.L. Wu, P.L. Fan, J.M. Hsu, and C.T. Lee, Design of ideal structures for lossless bends in optical waveguides by conformal mapping, J Lightwave Technol 14 (1996), 2604–2614.
8. M.D. Feit and J.A. Fleck, Jr., Computation of mode properties in optical fiber waveguides by a propagating beam method, Appl Opt 19 (1980), 1154–1164.
9. R. Baets and P.E. Lagasse, Calculation of radiation loss in integrated-optic tapers and Y-junctions, Appl Opt 21 (1982), 1972–1978.
10. M. Rangaraj, M. Minkata, and S. Kawakami, Low loss integrated optical Y-branch, J Lightwave Technol 7 (1989), 753–758.
11. S.M. Sze, VLSI technology, McGraw-Hill, New York, 1983.
12. H.K. Pulker, Characterization of optical thin films, Appl Opt 18 (1979), 1969–1977.
13. T. Tamir, Guided-wave optoelectronics, Springer-Verlag, Berlin, Germany, 1989.

IMAGE RECONSTRUCTION OF A THREE-DIMENSIONAL DIELECTRIC OBJECT USING A GRADIENT-BASED OPTIMIZATION

Haruyuki Harada,[1] Mitsuru Tanaka,[2] and Takashi Takenaka[3]
[1] Department of Electronic Control Engineering
Kagoshima National College of Technology
Kagoshima 899-5193, Japan
[2] Department of Electrical and Electronic Engineering
Oita University
Oita 870-1192, Japan
[3] Department of Electrical Engineering and Computer Science
Nagasaki University
Nagasaki 8521, Japan

Received 30 November 2000

ABSTRACT: *This paper presents an efficient reconstruction algorithm for three-dimensional scattering objects. The algorithm is an extension of previous work for the two-dimensional one, and is based on an optimization procedure. From the computer simulations, the proposed method is shown to yield satisfactory results, and to not be so sensitive to the presence of noise.* © 2001 John Wiley & Sons, Inc. Microwave Opt Technol Lett 29: 332–336, 2001.

Key words: *three dimensional; inverse scattering problem; cost functional; conjugate-gradient method*

I. INTRODUCTION

The electromagnetic characterization of scatterers has been an attractive research topic and of practical importance. Conventional diffraction tomography techniques are applicable to a weakly diffracting object within the first-order Born or Rytov approximation [1]. During the last two decades, a number of nonlinear inversion methods have been proposed to obtain good reconstructions even for cases where the two approximations break down [2–7].

In previous work [7], we presented an efficient method for solving the two-dimensional inverse scattering problem of